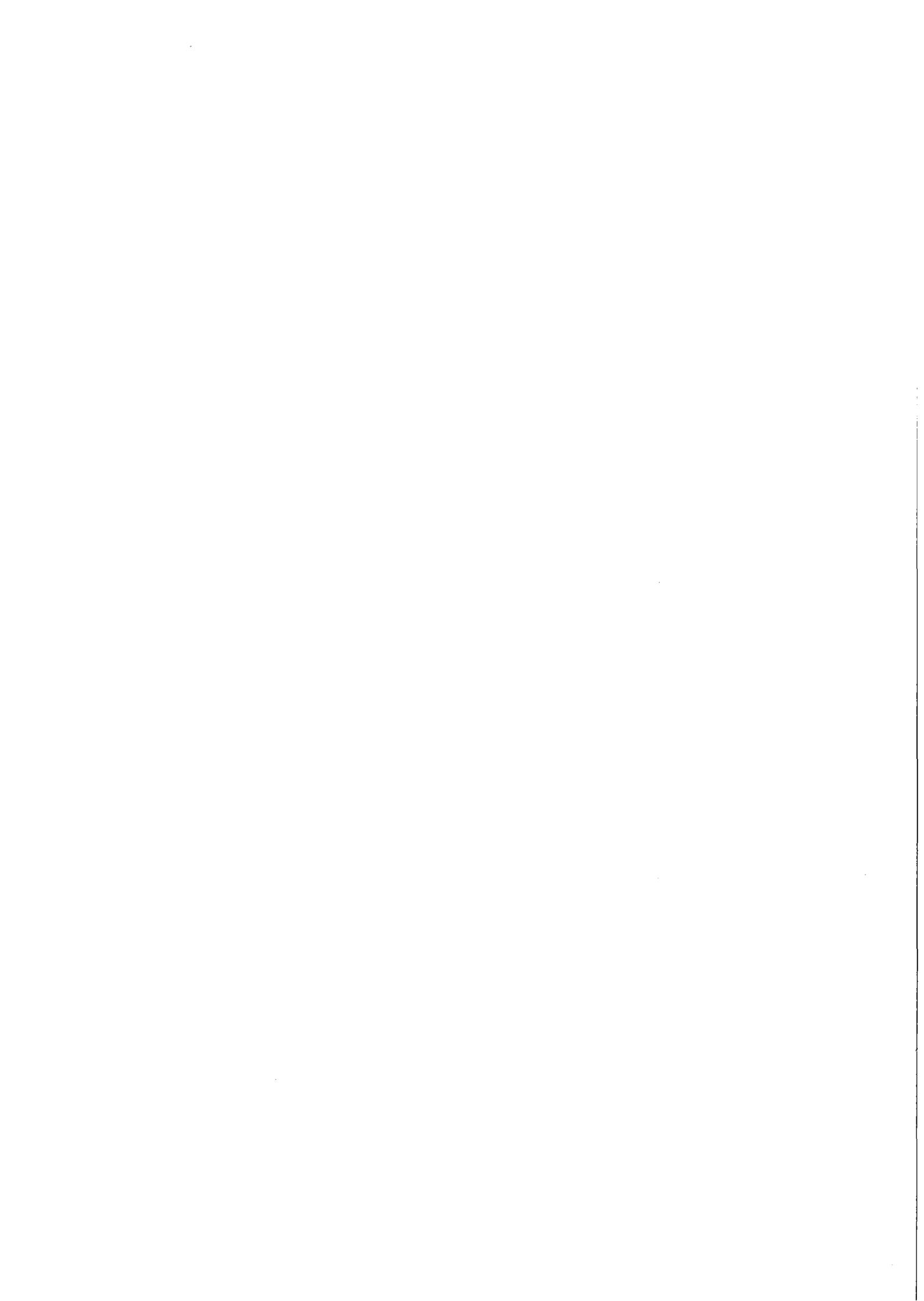


KfK 3772
Oktober 1984

High Temperature Vapor Pressures of Stainless Steel Type 1.4970 and of some other Pure Metals from Laser Evaporation

M. Bober, J. Singer
Institut für Neutronenphysik und Reaktortechnik
Projekt Schneller Brüter

Kernforschungszentrum Karlsruhe



KERNFORSCHUNGSZENTRUM KARLSRUHE
Institut für Neutronenphysik und Reaktortechnik
Projekt Schneller Brüter

KfK 3772

High Temperature Vapor Pressures of Stainless
Steel Type 1.4970 and of some other Pure Metals
from Laser Evaporation

M. Bober, J. Singer

Als Manuskript vervielfältigt
Für diesen Bericht behalten wir uns alle Rechte vor

Kernforschungszentrum Karlsruhe GmbH
ISSN 0303-4003

Abstract

For the safety analysis of nuclear reactors vapor pressure data of stainless steel are required up to temperatures exceeding 4000 K. In analogy to the classic boiling point method a new technique was developed to measure the high-temperature vapor pressures of stainless steel and other metals from laser vaporization. A fast pyrometer, an ion current probe and an image converter camera are used to detect incipient boiling from the time-temperature curve. The saturated-vapor pressure curves of stainless steel (Type 1.4970), being a cladding material of the SNR 300 breeder reactor, and of molybdenum are experimentally determined in the temperature ranges of 2800-3900 K and 4500-5200 K, respectively. The normal boiling points of iron, nickel, titanium, vanadium and zirconium are verified. Besides, spectral emissivity values of the liquid metals are measured at the pyrometer wavelengths of 752 nm and/or 940 nm.

Hochtemperatur-Dampfdrücke von Edelstahl Nr. 1.4970 und von einigen reinen Metallen aus Laser-Verdampfungsexperimenten

Zusammenfassung

Für die Sicherheitsanalyse von Kernreaktoren werden Dampfdruckdaten von Edelstahl bis zu Temperaturen über 4000 K benötigt. In Analogie zur klassischen Siedepunktmethode wurde ein neues Meßverfahren entwickelt, um die Hochtemperatur-Dampfdrücke von Edelstahl und anderen Metallen aus Laser-Verdampfungsexperimenten zu bestimmen. Aus dem zeitlichen Verlauf des Verdampfungsvorgangs wird der Siedebeginn mit Hilfe eines schnellen Pyrometers, einer Ionenstromsonde und einer Bildwandlerkamera ermittelt. Für den Edelstahl Nr. 1.4970, der als Hüllmaterial für den SNR 300 eingesetzt wird, und für Molybdän werden die Sättigungsdampfdruckkurven im Temperaturbereich von 2800-3900 K bzw. von 4500 - 5200 K experimentell bestimmt. Von Eisen, Nickel, Titan, Vanadium und Zirkon werden die normalen Siedepunkte verifiziert. Außerdem werden die gemessenen spektralen Emissionsgrade der flüssigen Metalle für die Pyrometerwellenlänge 752 nm und 940 nm angegeben.

Content

	page
Instroduction	1
Experimental method	3
Measurements	9
Discussion	21
Summary	25
References	26

Introduction

The safety analysis of nuclear reactors requires knowledge of the vapor pressure data of core materials up to high temperatures exceeding 4000 K. The accuracy requirements are not severe (1), however, experimental values are often completely lacking since conventional stationary measurement techniques fail at high temperatures. Therefore, diverse nonstationary measurement techniques were tried. Laser heating techniques were both used in a vacuum (2-4) and in a rarefied gas environment (5,6) to gain values of the high temperatures vapor pressure of oxide fuels. Besides, some in-pile tests were carried out with UO_2 (7,8). Up to now, only theoretical vapor pressure values exist of stainless steel cladding and structural materials (9) which were calculated on the basis of Raoult's law. For these calculations vapor pressure data of the steel components (10) need to be extrapolated from temperatures around the melting point up to 4000 K. The extrapolations cover six orders of magnitude in pressure so that an experimental verification of the high temperature values seems to be desirable.

The measurement techniques, based on laser surface evaporation of materials in a vacuum or rarefied gas, generally involve the necessity of complex gas-dynamic corrections (11,12). This can lead to rather large uncertainties in the evaluation of the desired saturation vapor pressures. Therefore a more straightforward technique has been used to get experimental vapor pressure data of liquid metals. In analogy to the classic boiling point method (13) the vapor pressure of the specimen material is approximated from laser vaporization experiments neglecting any additional corrections. The specimen surface is quasi-stationarily heated by a normal laser pulse under a defined inert gas atmosphere. At the onset of boiling a break occurs in the measured time-temperature curve which is caused by the discontinuous increase in the evaporation rate. In a series of experiments the boiling point of the specimen material can be confined within error bounds which fulfill the requirements of reactor safety analysis. Likewise one of the in-pile tests on UO_2 mentioned above (7), used the boiling point method.

The main difficulty with the laser experiments is the determination of the vaporization temperature. Optical pyrometry is without doubt feasible if the spectral emissivity of the incandescent liquid surface is known. However, in the stage of developed evaporation, when a luminous vapor plume has arisen, the pyrometric measurement might be disturbed by absorption of emitted thermal radiation in the supersaturated vapor plume (14). As soon as evaporation takes place the reactive vapor pressure displaces melt from the irradiation zone. This process flattens the radial temperature distribution in addition to the effect of evaporation cooling. But it has no significant influence on the evaporation behavior of the surface as long as no formation of deep craters occurs (15).

The laser power density must be limited to values below $10^5 - 10^6 \text{ W/cm}^2$ in order to achieve weak surface heating and to get normal evaporation conditions remaining close to equilibrium without significant superheat. At higher power densities ($10^6 - 10^9 \text{ W/cm}^2$) the equilibrium does not exist at the liquid-vapor phase boundary. The emission of thermoionic electrons and thermal ions results in the formation of a plasma layer which leads to screening of the irradiation zone and to plasma surface interaction (16). Superheating takes place which results in explosive break up of the metastable liquid surface (17).

Irradiation of a metal with a smooth millisecond laser pulse in the lower power-density regime leads to weak heating rates at minimum temperature gradients in the surface and allows thus clear detection of incipient boiling. Measurements have been performed on stainless steel and, in addition, on some unalloyed metals. The calculated saturated-vapor pressure curve of the steel, Typ 1.4970, being used as a cladding material in the SNR 300 breeder reactor, has been experimentally verified between 2800 and 3900 K.

Experimental method

The vaporization experiments have been carried out on the metallic specimens within a pressure chamber in which a distinct inert gas pressure of argon or krypton is maintained between 0.02 and 2 MPa.

Figure 1 shows schematically the experimental setup. A test-specimen of 6 mm in diameter and 1 mm thickness is located in the center of the pressure chamber which is equipped with several windows of fused silica. For millisecond times a Gaussian Nd:YAG laser beam is directed into the chamber and focussed on the specimen surface. At a moderate power density of some 10^5 W/cm² a surface spot of about 1 mm in diameter is weakly heated to temperatures around the boiling point. The increase of the central temperature of the irradiation zone is measured with a fast spectral pyrometer using the spectral emissivity of the molten material determined in preceding experiments. The boiling point can be found by correlating the time-temperature curve with the onset of strong evaporation detected by an image converter camera and an ion probe.

Up to 8 specimens are fixed on a revolving disk which allows changes of the specimens and new adjustments of the target position on the specimen surface during repeated laser bombardments. The Nd:YAG laser (LASAG, Model LAK 400/LV 480) consists of an oscillator/amplifier system delivering up to 20 Joules during a single pulse of 6 ms length as TEM₀₀. With an electro-optic modulator (Gsänger, Pockels cell Model DPZ8) the time-power profile of the pulse can be arbitrarily shaped under control of a programmable waveform generator (Wavetek, Model 175). In this way the heating rate of the material surface can be altered.

A spectral fast micropyrometer equipped with a silicon detector (EG+G, Type UV 15 B) is used to measure the radiance temperature of the molten material. By means of interference bandpass-filters (Oriel) the working wavelength can be chosen either at 752 or at 940 nm with bandwidths of 10 and 40 nm, respectively. The temperature resolution of the instrument is ± 1 K at 3000 K while the rise time is limited to 5 μ s. An integral sight telescope allows an accurate adjustment of the measurement spot being 0.13 mm in

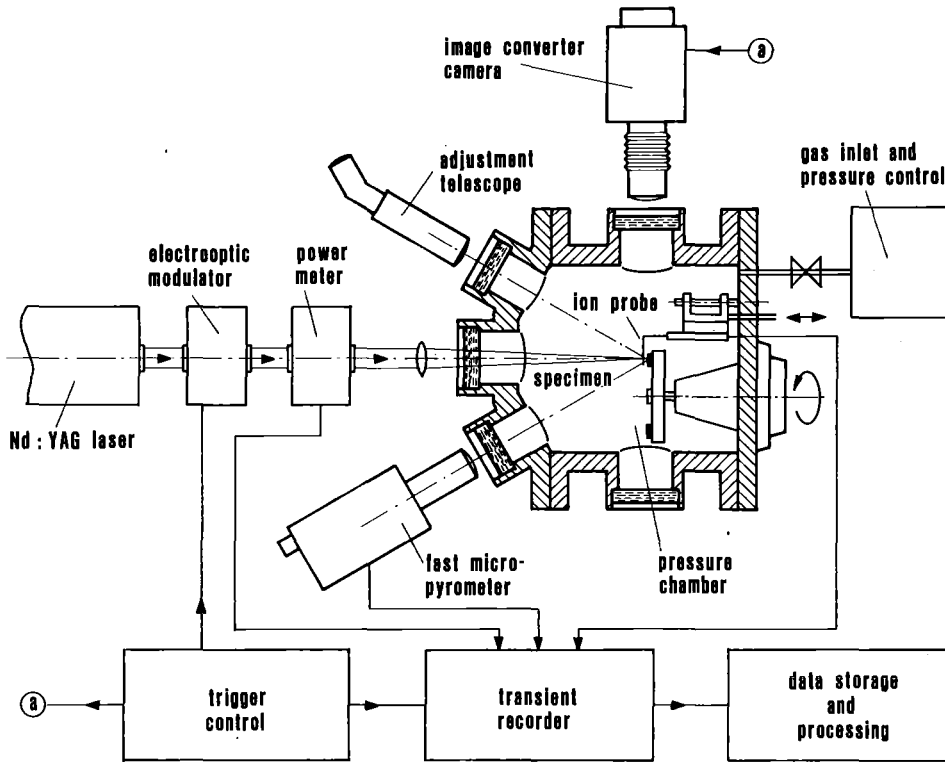


Fig.1. Principle of the measurement apparatus

diameter at a working distance of about 200 mm. The calibration of the pyrometer is repeatedly performed using two different gas-filled tungsten strip lamps (Osram, Type Wi 17G and G.E.C., Type 10/G). Both lamps were calibrated by the PTB (Physikalisch Technische Bundesanstalt, Braunschweig, West Germany) at a radiance temperature of 2400 K for 655 nm and have been converted to the working wavelengths using the known emissivity data of tungsten. The overall accuracy of the pyrometer, including the calibration error, is ± 15 K at a radiance temperature of 3000 K. However, the determination of the real surface temperature is subject to higher uncertainties which result from erroneous values of the spectral emissivity and from eventual absorption effects in the ambient atmosphere.

The extension of the luminous vapor plume is observed with a fast camera at several times during the laser pulse. For that purpose an image converter camera is used (STL/TRW, Model 1D) which produces a sequence of three frames on the scale of 2.9 to 1 at intervals of 0.5 ms. Provided the first picture is actuated at the onset of evaporation, the time elapsed up to the third picture is sufficient to make the expansion rate of the vapor plume clearly visible. Besides, an ion probe is placed in front of the specimen which serves to indicate the extension of the vapor being partly ionized. Symmetrical to the laser target spot the probe is adjusted at a chosen distance of about 1 mm from the surface. It consists of two parallel tungsten pins of 0.3 mm in diameter forming a fork with an inside width of 1.2 mm. Its open end is turned towards the camera. This shape of the probe allows an unhindered passage of the laser beam toward the surface and a clear sight of the vapor plume by the camera. With a voltage of -5V, applied between the probe and the specimen, an electric current signal is generated if positive metal ions get to the probe from the vapor plume.

Both the image converter camera and the ion probe allow to monitor the increase in the evaporation rate occurring near the boiling point. Also the corresponding development of the vapor plume can be associated with the measured time-temperature curve. At each experiment the time-temperature curve, the probe signal,

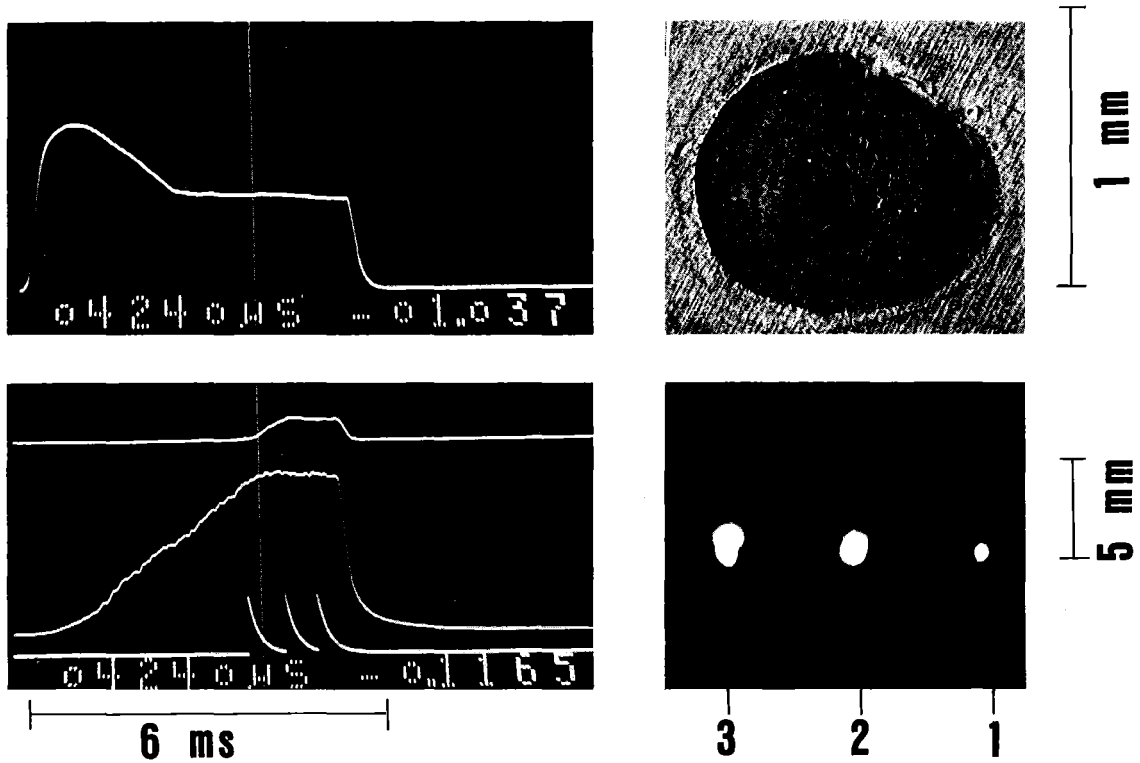


Fig.2. Measurement signals obtained on stainless steel (Type 1.4970) at an ambient pressure of 0.14 MPa of krypton. At left (from top to bottom): Oscillograms of the shaped laser pulse, ion probe signal, pyrometer signal, and trigger marks of the frames. At right: A photo of the refrozen surface of the laser heated zone with an indication of the pyrometer measurement spot, and (below) three successive frames of the image converter camera taken at intervals of 500 μ s (exposure time is 2 μ s).

the trigger marks of the frames, and the power history of the laser pulse are recorded and stored digitally for evaluation (Nicolet, Models 1090A and 2090A).

During a series of vaporization experiments a given inert gas pressure is established in the pressure chamber. The atomic mass of the inert gas is chosen to be similar to that of the emerging vapor. Step by step, the laser power is increased until strong evaporation appears which is detected by the ion probe and the camera. At the onset of enhanced evaporation a change or break occurs in the slope of the temperature-versus-time plot. This break is mainly caused by evaporation cooling which seems to proceed at the boiling temperature. From trial-and-error experiments an upper and lower bound is determined for the boiling point. An uncertainty arises from the fact that the temperature distribution is nonuniform across the laser irradiation zone. In the experiment evaluation the maximum temperature, measured in the center of the molten spot, is taken to be the boiling temperature.

At high power densities, laser bombardment can cause superheating of the surface layer which generally leads to explosive-like ejection of liquid droplets from the surface. Such a process is far away from evaporation equilibrium (17). Therefore, the heating rate must be chosen to be so moderate that surface evaporation will proceed at a condition close to the state of equilibrium. This was found to be the case if the heating rate of the surface does not exceed some 500 K/ms at temperatures above the melting point. Under these conditions, also the drift of the vapor plume can be considered not to disturb the evaporation equilibrium significantly. In general, repeated laser interaction with the same sample is possible without generating of a deep crater.

To illustrate the measurement method, Fig.2 gives an example of typical measurement signals obtained on stainless steel near the boiling point. From top to bottom, the oscillograms on the left hand side show the power history of the laser pulse, the ion probe signal, the pyrometer signal, and the trigger marks of the frames.

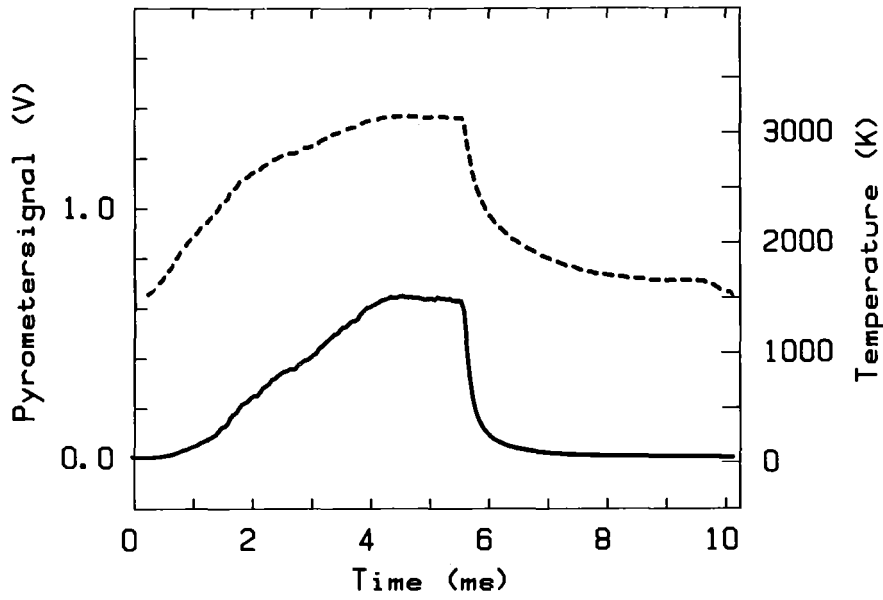


Fig.3. Pyrometer signal curve (full line) and the corresponding time-temperature curve (dashed line).

The plateau of the pyrometer signal, which coincides with the rise of the ion probe signal, denotes the onset of boiling. The upper right photo in Fig.2 shows the refrozen surface of the laser heated zone. The circle in the center of the picture indicates the size of the measurement spot of the pyrometer. Below, the frames of the image converter camera, being numbered in temporal succession from right to left, exhibit the development of the vapor plume. Figure 3 shows the time-temperature curve (dashed line) which results from evaluation of the pyrometer signal curve (full line). On the given linear temperature scale, the beginning of the plateau is less distinct but still well perceptible.

Measurements

Measurements have been performed on liquid stainless steel, iron, nickel, molybdenum, titanium, vanadium and zirconium. The saturated-vapor pressure curves of stainless steel (s.s.) and molybdenum have been experimentally determined in the temperature ranges of 2800 - 3900 K and 4500 - 5200 K, respectively. In case of the other metals the normal boiling points have been verified.

The stainless steel used in the experiments (Mat. no. 1.4970, DIN 17007) has the following composition in weight percent:

15.0 Cr, 15.1 Ni, 1.2 Mo, 1.7 Mn,
0.5 Ti, 0.5 Si, 0.1 C, remainder Fe.

For the unalloyed metals (supplied by Ventron GmbH/Alfa Products) the following purities have been specified (percent of metallic content): Iron (99.998), nickel (99.99), molybdenum (99.97), titanium (99.7), vanadium (99.5), and zirconium (99.2).

All metal vapor pressures have been measured with argon gas as well as krypton gas in the pressure chamber except molybdenum where the measurements have been performed only under krypton. Despite of different impurity contents of the two gases (Argon: 1 vpm oxygen, 1 vpm water and 1 vpm nitrogen; krypton: 2 vpm oxygen, 5 vpm water and 20 vpm nitrogen at maximum) no systematic differences could be detected with the two different gases.

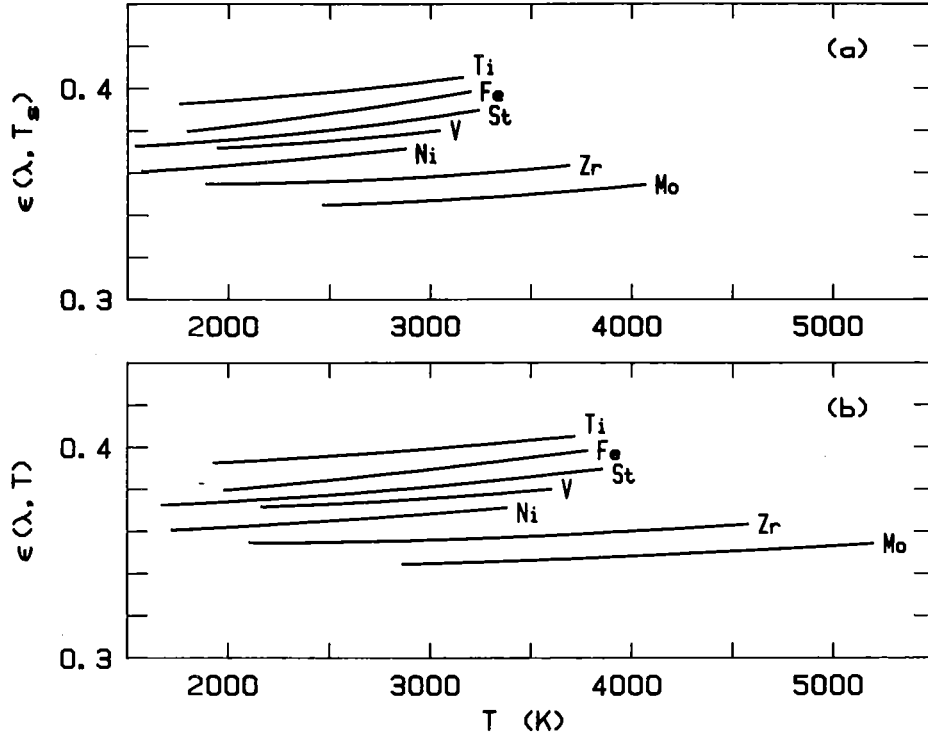


Fig.4. Spectral emissivities at 752 nm both plotted vs. the radiance temperature (a) and the real surface temperature (b).

Preceding the vaporization experiments, the spectral emissivity of each material was determined as a function of the temperature from reflectivity measurements at one wavelength, λ . These measurements were performed at 752 nm on molten specimen surfaces with an integrating-sphere laser reflectometer (18,19) in which laser beam heating of the sample material is used. An inert gas pressure was maintained in the reflectometer which corresponds to that, kept in the pressure chamber during the vaporization experiments. The desired spectral emissivity, $\epsilon(\lambda,T)$ depending on temperature, is obtained from the measured reflectivity, $\rho(\lambda,T)$, by the equation

$$\epsilon(\lambda,T) = 1 - \rho(\lambda,T). \quad (1)$$

At the pyrometer wavelength another single emissivity value has been deduced from the radiance temperature measured during the vaporization experiments at the known freezing point of the molten material. This value has been applied to adapt the temperature-emissivity curve, determined at 752 nm, to the equivalent curve needed for the pyrometer wavelength by assuming a similar temperature dependence.

Table 1 gives the spectral emissivity values, $\epsilon(\lambda,T)$, which have been determined from the radiance temperature, T_r , evaluated at the freezing point plateau of the time-temperature curves. The error margins of the emissivity values include the measurement errors of the radiance temperatures and the uncertainties in the given freezing point data (10,20,21). Table 2 contains the dependence of the emissivity values on the radiance temperature, derived from reflectivity measurements at 752 nm. The standard deviation of these measurements is within ± 0.01 . Figure 4 shows the spectral emissivity values both plotted versus the radiance temperature and the real surface temperature.

Owing to the dense absorption spectrum of iron, chromium and nickel in the visible spectral range, the pyrometric temperature measurement on steel could be disturbed by absorptions in the vapor plume. Therefore, the surface temperature of steel has been measured in the infrared at the wavelength of 940 nm to which the temperature dependence of the emissivity, being measured at 752 nm, has been

Table 1

Radiance temperatures, $T_r(f)$, and the spectral emissivities, ϵ , determined for two wavelengths, λ , at an angle of emission of 30° and the freezing point, $T(f)$.

Mat.	T(f) (K)		$\lambda = 752 \text{ nm}$				$\lambda = 940 \text{ nm}$			
			$T_r(f)$ (K)	SD ^a	ϵ	$\Delta\epsilon$ ^b	$T_r(f)$ (K)	SD	ϵ	$\Delta\epsilon$
s.s.	1685	Ref.20	1550	2	0.37_2	± 0.02	1515	2	0.36_0	± 0.02
Fe	1809	Ref.10	1658	2	0.38_0	$\pm 0.01_5$	1605	3	0.34_1	$\pm 0.01_5$
Ni	1726	Ref.10	1586	3	0.37_4	$\pm 0.01_5$	1538	2	0.33_8	$\pm 0.01_5$
Mo	2896	Ref.21	2478	4	0.33_0	± 0.01	2374	3	0.31_4	± 0.01
Ti	1943	Ref.10	1771	2	0.38_4	$\pm 0.01_5$	1726	3	0.37_1	$\pm 0.01_5$
V	2175	Ref.10	1956	2	0.37_2	± 0.02	1896	2	0.35_4	$\pm 0.01_5$
Zr	2125	Ref.21	1899	2	0.34_2	$\pm 0.01_5$	1844	3	0.33_4	± 0.01

^aStandard deviation of $T_r(f)$, ^berror margin of $\epsilon(\lambda, T)$

Table 2

Spectral emissivities as a function of the radiance temperature, T_r , at 752 nm, derived from reflectivity measurements at an angle of reflection of 30° in the given temperature range (cf. Fig.4a).

$$\epsilon(752\text{nm}, T_r) = A + Bt + Ct^2, \quad t = T_r - T_r(f)$$

Material	$T_r(f)$, (K)	A	$B \times 10^6$	$C \times 10^9$	T_r range, (K)
s.s. 1.4970	1550	0.373	5.15	2.93	1550 - 3300
iron	1658	0.380	10.6	2.09	1658 - 3200
nickel	1586	0.361	6.13	1.71	1586 - 2850
molybdenum	2478	0.345	3.26	1.79	2478 - 4100
titanium	1771	0.393	5.79	2.31	1771 - 3200
vanadium	1956	0.372	4.71	2.76	1956 - 3100
zirconium	1899	0.355	0.533	2.45	1899 - 3700

extrapolated. In case of stainless steel this means only a minor correction since emissivity varies only little with the wavelength at the freezing temperature (Table 1). A similar extrapolation of the emissivity values has been made for iron and nickel whose vaporization temperatures have been also measured at 940 nm. The temperature measurements on the other metals have been performed at 752 nm.

The laser vaporization experiments on stainless steel have been carried out under various inert gas pressures adjusted between 0.02 and 2 MPa. At each pressure up to 20 single experiments have been performed by applying slightly different laser power densities to ascertain the average temperature which corresponds to the boiling point. This evaluation generally succeeds within a standard deviation of ± 35 K. Fig. 5a,b shows examples of two series of measurement signals obtained at ambient gas pressures of 0.14 and 0.4 MPa. The signals illustrate the range in which the vaporization temperature should be located. The pyrometer signals (middle curve) and the probe signals (top curve) together with the frames of the image converter camera indicate the onset of surface boiling. At lower laser power densities, when the boiling point has not yet been reached, the frames of the image converter camera show no marked vapor plume development and the probe signal is lacking. At higher power densities, if the boiling temperature has been clearly exceeded, the frames indicate an intense vapor jet formation increasing with the heating rate. The in-between situation is demonstrated in the examples of Fig. 5a,b. In these two series of measurements the boiling point is measured to lie in the temperature range indicated at the three oscillograms. The frames reveal the distinct expansion rates of the vapor plumes rising to about 1 mm/ms, which help to determine the upper and lower bounds of the vaporization temperature.

At pressures exceeding 1 MPa the ion probe signal is delayed relative to the break in the temperature signal which makes the evaluation of the begin of boiling more uncertain. For this reason, measurements generally have been not attempted at pressures much above 1 MPa.

Figure 6 shows the resulting vapor pressure curve of liquid stainless steel (Type 1.4970) together with that of liquid molybdenum plotted in a $\log p$ vs. $1/T$ diagram. In the given temperature range the experimental points obtained for stainless steel (cf. Table 3) can be fitted by a straight line represented by the equation

$$\log p(\text{MPa}) = 5.237 - 19100/T(\text{K}). \quad (2)$$

The bars at the single points denote the standard deviation of the temperature evaluation. Additionally considering the errors of the temperature measurements arising from the uncertainties in the spectral emissivity values and from the pyrometer imprecision, the confidence limits which are indicated by the shadowed band along the curve have been obtained. These confidence limits imply errors of $\pm 55\text{K}$ at the normal boiling point of 3063 K of the steel and $\pm 75\text{ K}$ at the measured temperature of 3900 K , which correspond to inaccuracies of the vapor pressure values being less than $\pm 30\%$. It was not tried to express these uncertainties in the parameters of equation 2. Based on the Clausius-Clapeyron equation an average value of 366 kJ/mol for the heat of vaporization can be derived from the slope of the fit curve, which well agrees with the value of 361 kJ/mol obtained from theoretical extrapolations for the ss. Type 316 L (9). In comparison with the experimental points the dashed line is given which represents a theoretical vapor pressure curve calculated on the basis of Raoult's law from lower temperature component data (22).

The dotted line shown in Fig.6 is a boundary line which has been measured for superheated steel. Vaporization experiments performed on liquid steel at heating rates of some 3000 K/ms (with incident laser power densities of about 10^6 W/cm^2) have superheated the surface and led to an explosive-like break up of the metastable liquid layer. Fig.7 shows two examples of temperature signals obtained from a superheated liquid steel surface. The obtained superheat temperature depends on the ambient gas pressure which here amounts to approximately half the saturated-vapor pressure (23). The boundary line of superheat has been found to be reproducible in the whole pressure range from 0.02 to 2 MPa during a series of experiments.

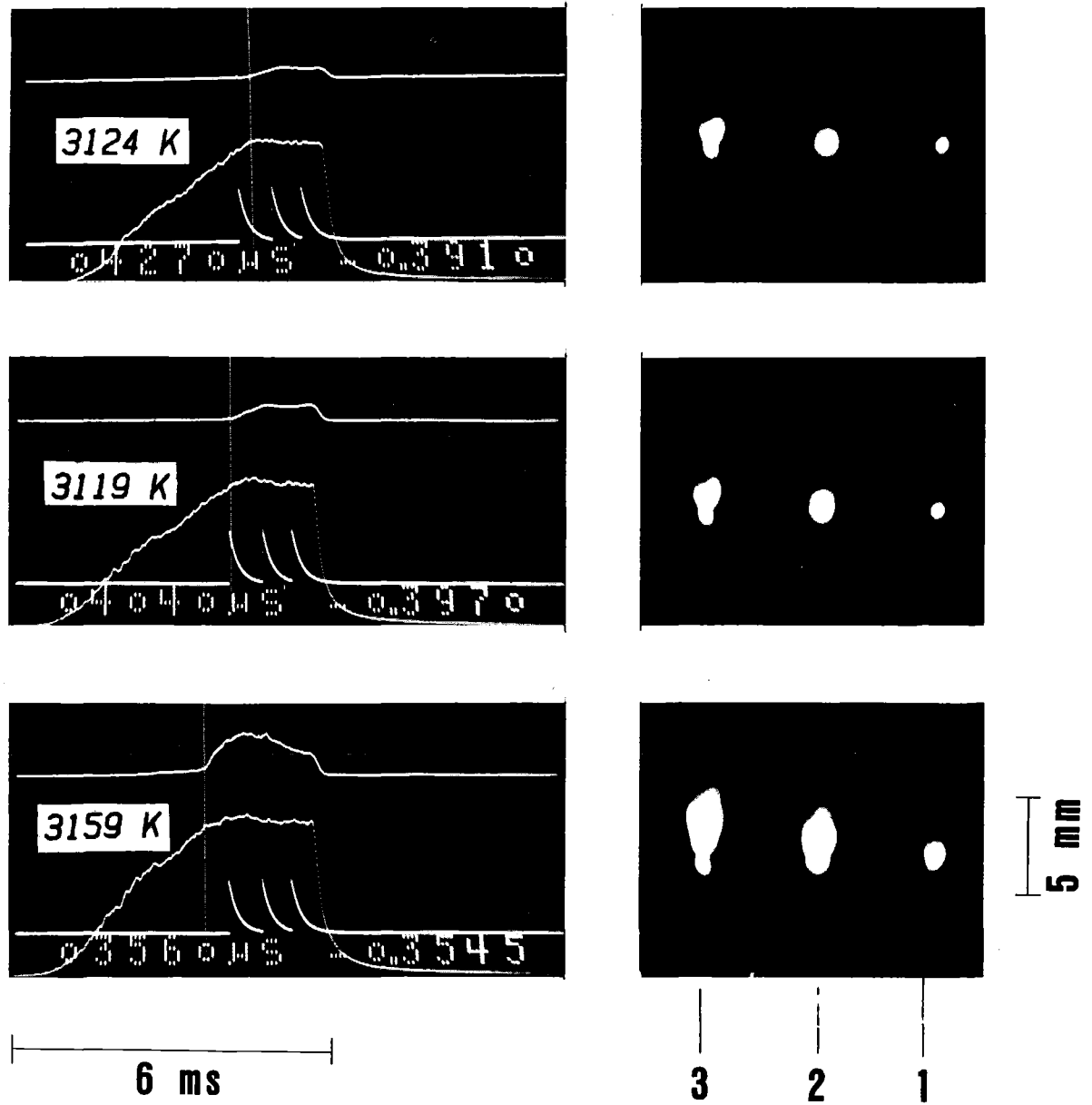


Fig.5a Measurement signals of three experiments obtained on stainless steel (Type 1.4970) at 0.14 MPa of krypton (cp. note on Fig.2). The vaporization temperatures are indicated at the pyrometer-signal traces.

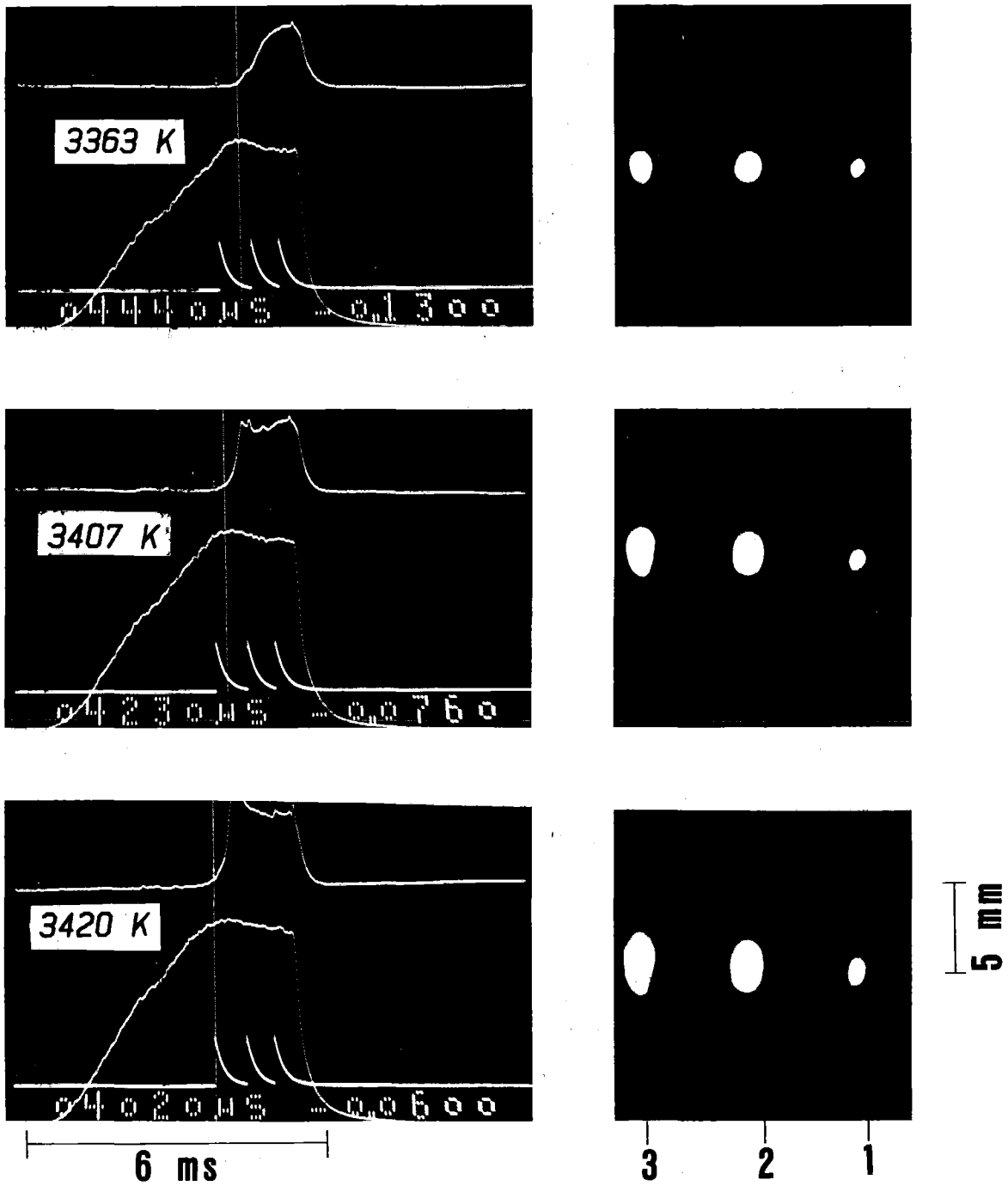


Fig.5b Measurement signals of three experiments obtained on stainless steel (Type 1.4970) at 0.4 MPa of krypton (cp. note on Fig.2). The vaporization temperatures are indicated at the pyrometer-signal traces.

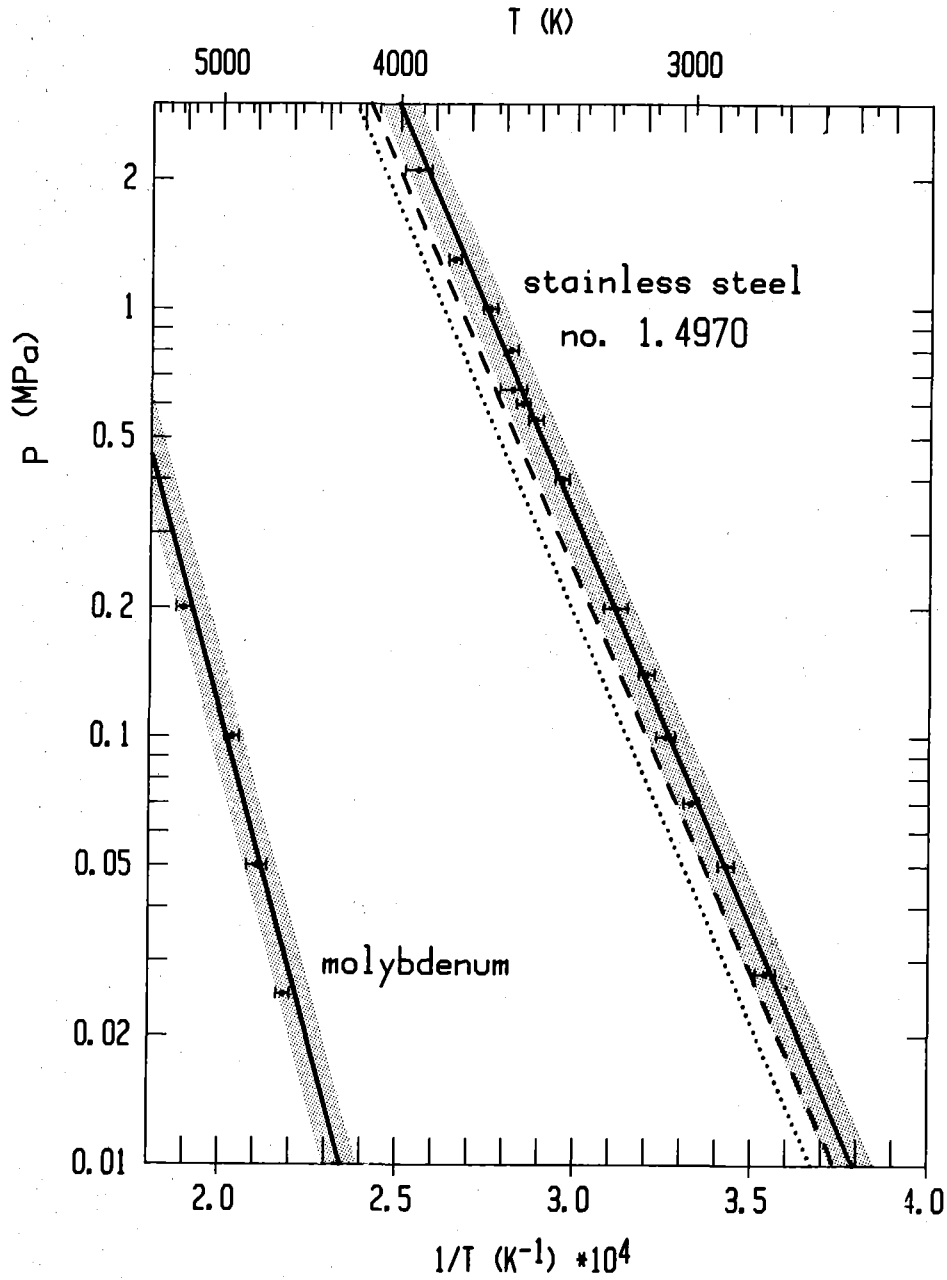


Fig.6. Vapor pressures of liquid stainless steel (Type 1.4970) and of liquid molybdenum as functions of the reciprocal temperature. The full lines fit the experimental points. The dashed line represents a theoretical extrapolation from lower temperature component data of steel, and the dotted line is a boundary experimentally found for superheat of steel.

Table 3

Experimental equilibrium vapor pressures obtained for s.s.1.4970.

vapor pressure (MPa)	temperature (K)
2.10	3924
1.30	3769
1.00	3630
0.80	3555
0.65	3545
0.60	3509
0.55	3466
0.40	3377
0.20	3213
0.14	3124
0.10	3070
0.07	3003
0.05	2917
0.028	2825

Table 4

Experimental equilibrium vapor pressures obtained for molybdenum.

vapor pressure (MPa)	temperature (K)
0.20	5278
0.10	4916
0.05	4750
0.025	4586

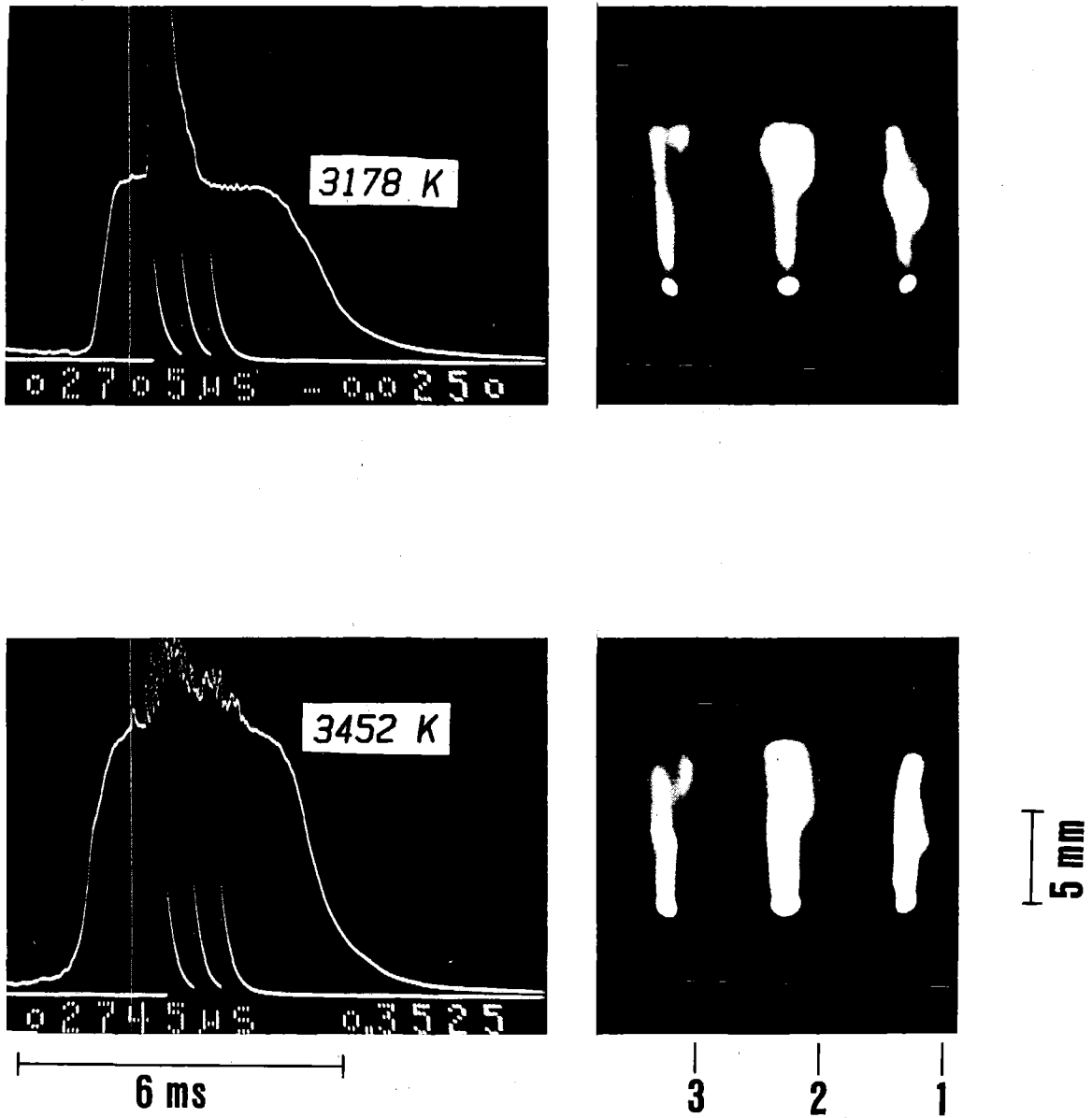


Fig. 7. Pyrometer signals from a superheated steel surface exhibiting an explosive break up of the liquid. The ambient gas is argon of 0.1 MPa (top) and 0.3 MPa (bottom). The corresponding frames of the image converter camera (cp. note on Fig.2) show the intense vapor jet formation. The maximum extension of the plumes is limited by the size of the frames.

For the purpose of comparison, the vapor pressure curve of molybdenum has been measured in laser vaporization experiments at temperatures around the normal boiling point. The result is shown in Fig.6 where the shadowed band again denotes the confidence limits of the temperature evaluation. The experimental points (cf. Table 4), including the vapor pressure value at the melt temperature (10), can be fitted by the equation

$$\log p(\text{MPa}) = 5.147 - 30500/T(\text{K}) \quad (3)$$

The slope of this straight line corresponds to a tentative value for the heat of vaporization of 584 kJ/mol which is in good agreement with the theoretically extrapolated value of 590 kJ/mol (21).

Table 5 contains values of the normal boiling points of molybdenum and the other metals, which have been experimentally verified. Most of them satisfactorily agree with the calculated values given in literature (10,21,24). The table include the measured radiance temperatures and the spectral emissivity values which have been used in temperature evaluation. The given error margins proceed from error propagation calculations.

Discussion

The main uncertainty in the measured p-T relation arises from the errors of the pyrometric temperature measurements, which are largely caused by the uncertainties of the spectral emissivity values. An additional uncertainty in the vaporization temperature stems from the radial temperature gradient in the laser irradiation zone. It is felt however that this uncertainty is less important than that of the temperature measurement. It diminishes when the laser is operated at a suitable mode which flattens the spatial power density profile in the laser focal spot. Besides, during weak laser heating, radial liquid flow and heat conduction take place which additionally flattens the temperature distribution in the central region of the irradiation zone.

Table 5

Normal boiling points, $T(b)$, of the examined metals ($p = 0.1$ MPa).

λ is the pyrometer wavelength. $T_r(b)$ and $\epsilon(\lambda, T_r)$ are the measured radiance temperatures and the emissivity values, respectively.

Material	experimental values				calculated values	
	λ (nm)	$T_r(b)$ (K)	$\epsilon(\lambda, T_r)$	$T(b)$ (K)	$T(b)$ (K)	
s.s.1.4970	940	2560 \pm 26	0.37 ₃	3063 \pm 55	(3090	Ref. 9) ^a
iron	940	2603 \pm 13	0.35 ₅	3156 \pm 38	3148	Ref. 10
					3136	Ref. 21
nickel	940	2599 \pm 19	0.35 ₀	3160 \pm 43	3187	Ref. 10
					3183	Ref. 24
molybdenum	752	3885 \pm 36	0.33 ₈	4962 \pm 77	4912	Ref. 10
					4957	Ref. 21
titanium	752	3040 \pm 32	0.39 ₅	3564 \pm 53	3562	Ref. 10
					3592	Ref. 21
					3563	Ref. 24
vanadium	752	3091 \pm 19	0.38 ₁	3659 \pm 48	3682	Ref. 10
					3694	Ref. 21
					3623	Ref. 24
zirconium	752	3770 \pm 34	0.35 ₂	4732 \pm 78	4682	Ref. 10
					4777	Ref. 21
					4578	Ref. 24

^a Calculated value for the boiling point of s.s. Type 316L

The change in the slope of the time-temperature curve, indicating incipient boiling, is primarily caused by evaporation cooling of the liquid surface. Only the further development of the temperature plateau, as shown in Figs. 2 and 5, can be influenced by absorption in the vapor cloud which however does not confuse the evaluation at this stage. The vaporized fast molecules are slowed down by collisions with the inert gas atoms, and thus the vapor cloud becomes supersaturated. During the stage of developed evaporation the molecules partly recondense and form clusters which leads to scattering and absorption effects of the thermal radiation emitted from the surface. The incident laser radiation likewise becomes screened to some extent. As a result, the temperature measurement can be assumed to be reliable up to the onset of vapor cloud expansion which starts at temperatures close to the boiling points. At higher temperatures the pyrometric measurement becomes increasingly uncertain.

It thus appears that under the given experimental conditions, evaporation takes place at a state close to equilibrium. The inert gas atmosphere above the liquid surface hinders evaporation to such a degree that considerable backscattering of the vapor molecules occurs for comparable masses of vapor and inert gas atoms (25). Diffusion governs the development of the vapor plume. The numerous collisions of the vapor molecules with the gas atoms impede a gas-dynamic flow-off. The diffusion rates prevailing in the hot vapor-gas mixture are several times higher than those in the cold gas. This can be demonstrated by the theoretical concentration-distance curves of Fig.8 calculated for one-dimensional diffusion (26,27) of Fe-atoms in a semi-infinite medium of argon or krypton at a diffusion time of 1 ms. The vapor plume initially does not disperse. Slowing down of the fast vapor molecules takes place at the boundary of the hot vapor plume by generating recoils in the gas atmosphere within a distance of some mean free paths (28). So the expansion of the vapor plume can be assumed to be mainly caused by continuous evaporation at the sample surface. The development of the vapor plume, which is detected by the ion probe and the image converter camera, exhibits a measure for the onset of strong evaporation at the boiling point.

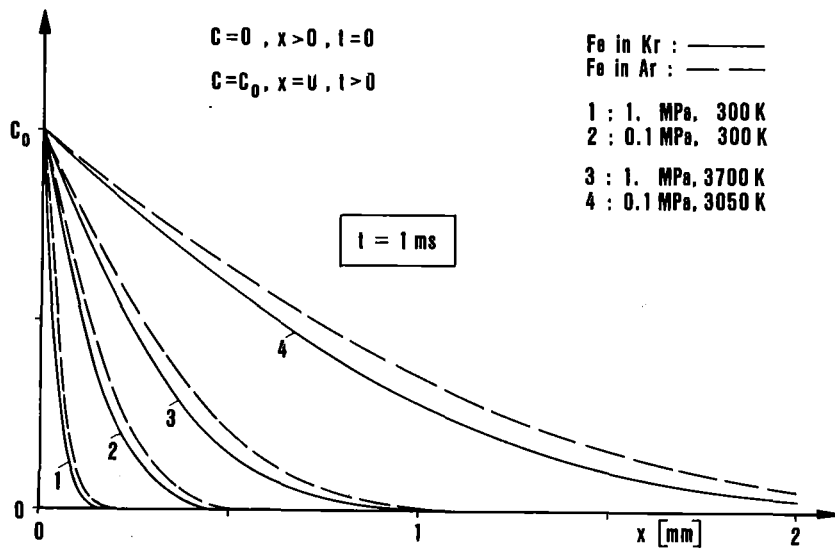


Fig.8. Theoretical concentration-distance curves /26/ calculated for one-dimensional diffusion of Fe-atoms in a semi-infinite medium of argon or krypton at $t=1$ ms. Diffusion coefficients are taken from a hard-sphere-model /27/. The boundary concentration is held constant ($C=0$) at $x=0$. The gas pressures are 0.1 and 1 MPa. Temperatures are the room temperature and the corresponding boiling temperatures of steel.

Summary

This work resulted in new experimental information on the saturation vapor pressure of liquid stainless steel. The obtained precision of the measurement method satisfies the requirements of reactor accident analysis. Within the given error margin, the measured vapor pressure values of stainless steel exceed the previous theoretical extrapolations by about 30%. The feasibility of the method could be demonstrated by the verification of the normal boiling points of various metals, covering a wide range of vaporization temperatures. Even at such high temperatures as 5000 K the theoretically calculated boiling point and the slope of the saturated-vapor pressure curve of molybdenum could be satisfactorily verified.

The measurement technique was found to be applicable up to temperatures of 5000 K provided vapor cloud densities are not too high. Although clear pressure bounds cannot be defined for the application of the experimental method, practical limits are 0.01 and 1 MPa. Outside these pressure limits the detection of boiling becomes difficult. Within the given pressure range the method is simple and allows to gain high temperature vapor pressure data of metals. Further improvements are possible by achieving more reliable spectral emissivity measurements which decisively determine the accuracy of temperature evaluation.

Acknowledgement

The authors wish to thank W. Breitung for helpful discussions and for reading the manuscript, R. Eggmann for development of the electronic equipment and S. Gaukel for mechanical constructions.

References

- /1/ M.G. Stevenson et al.,
An Overview Assessment of Energetic Core Disruptive Accidents,
Proc. Int. Meeting on Fast Reactor Safety Technology, Vol.3,
Seattle, Wash., USA (1979) p.1406.
- /2/ M. Bober, W. Breitung, H.U. Karow, K. Schretzmann,
Evaporation Studies of Liquid Oxide Fuel at Very High Temperatures
Using Laser Beam Heating, Report KfK-2366, Kernforschungszentrum
Karlsruhe, (1976).
- /3/ M. Bober, W. Breitung, H.U. Karow,
Thermodynamic Calculation and Experimental Determination of the
Equation of State of Oxide Fuels up to 5000 K, Report KfK-2689,
Kernforschungszentrum Karlsruhe, (1978).
- /4/ J.F. Babelot, G.D. Brumme, P.R. Kinsman, R.W. Ohse,
Vapour Pressure Measurement Over Liquid UO_2 and $(U,Pu)O_2$ by
Laser Surface Heating up to 5000 K, Atomwirtschaft-Atomtechnik 12,
(1977) 387.
- /5/ H.C. Tsai, A. Covington, D.R. Olander,
Laser Vaporization of UO_2 , Report LBL-6016, UC-13, Materials
and Molecular Research Division, Lawrence Berkeley Laboratory,
Berkeley, Cal., USA (1976) p.188.
- /6/ R.W. Ohse, J.F. Babelot, A. Frezzotti, K.A. Long, J. Magill,
Equation of State of Uranium Oxide: Mach-Disk Investigation
of Transient Laser-Induced Vaporization of UO_2 up to 5000 K,
High Temperatures - High Pressures 12, (1980) 537.
- /7/ R. Limon, G. Sutren, P. Combette, F. Barbry,
Equation of State of Non Irradiated UO_2 , Proc. ANS/ENS Topical
Meeting on Reactor Safety Aspects of Fuel Behavior, Vol. 2,
Sun Valley, Idaho, USA (1981) p.576.

- /8/ K.O. Reil, W. Breitung,
High Precision In-Pile Measurement of the Vapor Pressure Over
High-Purity UO_2 , Proc. L.M.F.B.R. Safety Topical Meeting,
Vol.4, Lyon, France (1982) p.631
- /9/ C.S. Kim,
Thermophysical Properties of Stainless Steel, Report ANL-75-55,
Argonne National Laboratory, Argonne Ill., USERDA (1975).
- /10/ R. Hultgren et al.
Selected Values of the Thermodynamic Properties of the Elements,
American Society for Metals, Metals Park, Ohio, USA (1973).
- /11/ Yu.V. Afanas'ev, O.N. Krokhin,
Vaporization of Matter Exposed to Laser Emission, Soviet
Physics JETP 25, (1967) 639.
- /12/ S.I. Anisimov et al.,
Effect of Powerful Light Fluxes on Metals, Sov. Phys. Tech.
Phys. 11, (1967) 945.
- /13/ J.L. Margrave,
The Characterization of High-Temperature Vapors, John Wiley
a.Sons, Inc., New York (1967) p.74.
- /14/ S.V. Gaponov, A.A. Gudkov, A.A. Fraerman,
Condensation in Gas Flows During Laser Vaporization of Materials,
Sov. Phys. Tech. Phys. 27, (1982) 1130.
- /15/ B.M. Zhiryakov, A.I. Korotchenko, N.I. Popov, A.A. Samokhin,
Influence of Hydrodynamic Perturbation on Laser Evaporation
of Metals with a Phase Interface, Sov. J. Quantum Electron. 13,
(1983) 763.
- /16/ F. Schwirzke,
Unipolar Arcing, a Basic Laser Damage Mechanism, Report
NPS-61-83-008, Naval Postgraduate School, Monterey, Cal., USA
(1983).

- /17/ B.M. Kozlov, B.B. Krynetskii, A.A. Samokhin,
Evaporation of Metastable Liquid, Sov. J. Quant. Electron.,
4, (1975) 1303.
- /18/ M. Bober, H.U. Karow,
Measurements of Spectral Emissivity of UO_2 Above the Melting
Point, Proc. 7-th Symp. on Thermophysical Properties, NBS
Gaithersburg, Md., ASME, USA (1977) p.344.
- /19/ K. Wagner,
Die Bestimmung der optischen Stoffdaten von Schmelzen aus Uran-
carbid und Thoriumcarbid, Report KfK-3588, Kernforschungszentrum
Karlsruhe, (1983).
- /20/ P. Nikopoloulos, B. Schulz,
Density, Thermal Expansion of Stainless Steel and Interfacial
Properties of UO_2 - Stainless Steel Above 1690 K, J. Nucl.
Mater. 82, (1979) 172.
- /21/ D.R. Stull, H. Prophet,
JANAF Thermochemical Tables, 2nd Ed., NSRDS-NBS37, U.S. Depart-
ment of Commerce (1971), and Supplements, M.W. Chase, et al.,
J. Phys. Chem. Ref. Data 4, No.1 (1975) and 11 No.3 (1982).
- /22/ K. Thurnay,
Thermophysikalische Eigenschaften von Edelmetallen,
PSB-Vierteljahresbericht, Report KfK-1276/1, Kernforschungs-
zentrum Karlsruhe, (1976) p.123-17.
- /23/ N.V. Karlov, B.B. Krynetskii, V.A. Mishin, A.A. Samokhin,
Metastability of Liquid Phase Under Conditions of Developed
Evaporation of Condensed Media, JETP Letters 19, (1974) 68.
- /24/ O. Kubaschewski, E.L. Evans, C.B. Alcock,
Metallurgical Thermochemistry, 5th Ed., Pergamon Press, N.Y. (1979).

- /25/ Y.P. Pao,
Evaporation in a Vapor-Gas Mixture, J. Chem. Phys. 59,
6688 (1973).
- /26/ J. Crank,
The Mathematics of Diffusion, Clarendon Press, Oxford (1975)
p. 20.
- /27/ S. Chapman, T.G. Cowling,
The Mathematical Theory of Non-Uniform Gases, Cambridge
University Press (1953).
- /28/ M.M.R. Williams,
The Slowing Down of Fast Atoms in a Uniform Gas, Rarefied
Gas Dynamics (J.L. Potter Ed.), Vol. 51, Part 2, American
Institute of Aeronautics and Astronautics, N.Y., USA (1977)
p. 679.